Acta Crystallographica Section D
Biological Crystallography
ISSN 0907-4449

Structure of alcohol dehydrogenase from *Entamoeba histolytica*

Linda J. W. Shimon,[a]* Edi Goihberg,[b] Moshe Peretz,[b] Yigal Burstein[b] and Felix Frolow[c]

[a]Department of Chemical Research Support, The Weizmann Institute of Science, Rehovot 76100, Israel, [b]Department of Organic Chemistry, The Weizmann Institute of Science, Rehovot 76100, Israel, and [c]Department of Molecular Microbiology and Biotechnology, The Daniella Rich Institute for Structural Biology, Tel Aviv University, Ramat Aviv 69978, Israel

Correspondence e-mail: linda.shimon@weizmann.ac.il

Received 6 January 2006
Accepted 13 March 2006

PDB Reference: alcohol dehydrogenase, 1y9a, r1y9asf.

The structure of the apo form of alcohol dehydrogenase from a single-cell eukaryotic source, *Entamoeba histolytica*, has been determined at 1.8 Å. To date, bacterial and archeal alcohol dehydrogenases, which are biologically active as tetramers, have crystallized with tetramers in the asymmetric unit. However, the current structure has one independent dimer per asymmetric unit and the full tetramer is generated by application of the crystallographic twofold symmetry element. This structure reveals that many of the crystallization and cryoprotection components, such as cacodylate, ethylene glycol, zinc ions and acetate, have been incorporated. These crystallization solution elements are found within the molecule and at the packing interfaces as an integral part of the three-dimensional arrangements of the tetramers. In addition, an unexpected modification of aspartic acid to *O*-carboxysulfanyl-4-oxo-L-homoserine was found at residue 245.

1. Introduction

Alcohol dehydrogenases (ADHs; EC 1.1.1.1) catalyze the reversible oxidation of alcohols to the corresponding aldehydes or ketones utilizing the nicotinamide cofactors NAD(H) and NADP(H). They are ubiquitous enzymes found in nearly all classes of living organisms and representative structures of alcohol dehydrogenases from all three branches of life, prokaryotic, archeal and eukaryotic, are known. ADHs are organized by size into three main types: enzymes with chains of less than 250 residues (short chains) and without any metal ions, medium-chain zinc-containing enzymes of approximately 350 residues per chain (class II) and long-chain enzymes of more than 385 residues per chain (Danielsson *et al.*, 1994). Class II medium-chain zinc-dependent ADHs are biologically active either as homotetramers in bacteria, archaea and yeast or as homodimers in plants and vertebrates.

The three-dimensional structures of ADHs from a variety of sources (bacteria, archaea, fungi, plants and mammals) have previously been determined, with horse liver ADH being the best known example of this class (Eklund *et al.*, 1977; Pietruszko, 1975). In the tetrameric class, X-ray crystallographic structures have been determined for ADHs from the bacteria *Thermoanaerobacter brockii* (TbADH), *Clostridium beijerinckii* (CbADH; Korkhin *et al.*, 1998), *Escherichia coli* (Karlsson *et al.*, 2003) and *Pseudomonas aeruginosa* (PaADH; Levin *et al.*, 2004) and from the archaea *Sulfolobus solfataricus* (SsADH; Esposito *et al.*, 2002) and *Aeropyrum pernix* (Guy *et al.*, 2003).

The alcohol dehydrogenase from the eukaryotic single-cell parasite *Entamoeba histolytica* (EhADH) is a NADP(H)-dependent homotetrameric class II enzyme with one catalytic

Table 1
Crystallographic data and X-ray refinement statistics.

Values in parentheses are for the outer resolution shell.

Data collection	
Crystal	
Space group	$C222_1$
Temperature (K)	100
Unit-cell parameters (Å)	a = 76.89, b = 234.14, c = 96.24
Internal scaling	
Resolution (Å)	20–1.81 (1.83–1.81)
Reflections measured	181235
Unique reflections	70422
Completeness (%)	92.6 (95.9)
Average $I/\sigma(I)$	13.79 (1.88)
R_{sym}†	0.051 (0.486)
Wilson B factor	20.91
Refinement statistics	
R_{cryst}	0.155 (0.216)
R_{free} (5% of data)	0.186 (0.252)
No. of atoms	
Protein	6259
Water	788
Other	58
Average B values (Å^2)	
Protein	32.44
Water	45.07
Other	33.32
R.m.s.d.s. from target geometry	
Bond lengths (Å)	0.008
Bond angles (°)	1.390
Ramachandran plot statistics	
Residues in most favoured regions (%)	89.7
Residues in additional allowed regions (%)	10.3
Residues in generously allowed regions (%)	0.0
Residues in disallowed regions (%)	0.0

† $R_{sym} = \sum |I_i - \langle I \rangle| / \sum |\langle I_i \rangle|$.

zinc per monomer. The enzyme is active at elevated temperatures ($T^{1/2}_{60\,min}$ = 350 K; Bogin *et al.*, 1998) and catalyzes the reversible conversion of secondary alcohols to ketones. It has 360 residues per chain and is highly homologous (with approximately 62–75% sequence identity) to the functionally related tetrameric bacterial alcohol dehydrogenases TbADH and CbADH.

In previous studies, the EhADH gene has been cloned and overexpressed in *E. coli* and the protein has been crystallized (Shimon *et al.*, 2002). Here, we present the three-dimensional X-ray crystal structure of the apoenzyme EhADH at 1.8 Å resolution. The overall structure of this alcohol dehydrogenase from a single-celled eukaryotic source is similar to that of the previously determined homologous bacterial enzymes, but the details of the structure provide new insights into the symmetry of the tetrameric organization and arrangement of the dimer interfaces as well as the influence of the crystallization solute on the molecular and crystalline structure.

2. Experimental

2.1. Crystallization, data collection and structure solution

The 40 kDa recombinant protein consisting of the 360-residue alcohol dehydrogenase from *En. histolytica* was overexpressed in *E. coli* and purified as previously described (Goihberg, 2001; Peretz *et al.*, 1997; Samuelson *et al.*, 1992). Crystals were grown using the hanging-drop vapour-diffusion method at 291 K. In the final conditions for crystallization, 10 µl apo EhADH stock solution (11.5 mg ml^{-1} protein, 25 m*M* Tris–HCl, 50 m*M* NaCl, 0.1 m*M* dithiothreitol, 50 m*M* $ZnCl_2$ pH 7.5) was mixed with 1 µl reservoir solution [14%(*w*/*v*) PEG 8K, 300 m*M* magnesium acetate, 200 m*M* cacodylate buffer pH 6.5].

Table 2
Hydrogen-bonding interactions.

Residue	Atom	Residue	Atom	Distance (Å)
*A*98	O	*A*364	EDO O2	2.57
*A*99	Tyr OH	*C*289	His NE2	2.95
*A*102	His NE2	*C*287	His ND1	2.84
*A*271	O	*C*278	Arg NE	2.69
*A*272	O	*C*278	N	2.95
*A*274	O	*C*276	N	2.97
*A*274	N	*C*276	O	2.71
*A*276	O	*C*274	N	2.71
*A*276	N	*C*274	O	2.97
*A*278	N	*C*272	O	2.95
*A*283	O	*C*268	N	2.95
*A*284	O	*C*264	Asn ND2	2.87
*A*287	N	*C*292	O	2.80
*A*287	His NE2	*C*157	His NE2	2.90
*A*287	His ND1	*C*102	His NE2	2.84
*A*289	His ND1	*C*291	His ND1	2.99
*A*289	His NE2	*C*99	Tyr OH	2.95
*A*290	N	*C*290	O	2.96
*A*291	His ND1	*C*289	His ND1	2.99
*A*291	His NE2	*A*261	Asp OD1	2.76

2.2. Data collection

Prior to data collection, the crystals were transferred into a cryoprotectant solution mimicking growth conditions with the addition of 25%(*w*/*v*) ethylene glycol. Crystals were mounted in a rayon loop and flash-cooled in a stream of cold nitrogen at 100 K for data collection at beamline ID14-1 at ESRF. A full native data set to 1.8 Å was collected as 0.5° oscillation frames with 30 s per pass and two passes per frame at a distance of 120 mm using a MAR Research 165 CCD detector and a wavelength of 0.934 Å. Data were processed and reduced using the *HKL* suite (Otwinowski & Minor, 1997). The crystal and data parameters are summarized in Table 1.

2.3. Structure solution

The initial structure of EhADH was determined by molecular replacement using *AMoRe* (Navaza, 1994) as implemented in the *CCP*4 suite (Collaborative Computational Project, Number 4, 1994) utilizing a coordinate set from the nearly 75% homologous CbADH (PDB code 1ped; Korkhin *et al.*, 1998) as a search model. EhADH contains a dimer in the asymmetric unit and molecular replacement was performed to 3.0 Å, yielding a solution with a correlation coefficient of 36.5% and an R factor of 49.9%. A random subset of the data (5%) was set aside for cross-validation and assessment of the refinement. The total omit-map procedure was applied using *CNS* (Brünger *et al.*, 1998) to eliminate the bias from our

molecular-replacement model and to return an electron-density map which better described our sequence. The non-conserved residues were then built into a total omit electron-density map using the program *O* (Jones *et al.*, 1991).

2.4. Refinement

The structure was subsequently refined using *CNS* (Brünger *et al.*, 1998) and *SHELXL*97 (Sheldrick & Schneider, 1997). At each stage, manual rebuilding was performed using *O* (Jones *et al.*, 1991) and quality assessment was performed using *PROCHECK* (Laskowski *et al.*, 1993) and *WHATIF* (Vriend, 1990). The final stages of refinement were performed using *REFMAC* (Murshudov *et al.*, 1997) as implemented in *CCP*4, together with *COOT* (Emsley & Cowtan, 2004) for manual rebuilding and analysis. Water molecules were added automatically using *ARP*/*wARP* (Lamzin & Wilson, 1993; Lamzin *et al.*, 2001) as implemented in *CCP*4*i* (Potterton *et al.*, 2003). Small solute molecules were located and identified by manual inspection of the difference electron-density maps and added manually. Refinement in *REFMAC* allows for the anisotropic motion of rigid bodies, described as TLS parameters (Winn *et al.*, 2003). The target geometry parameters used in refinement were from Engh & Huber (1991) for the protein and from the HIC-Up database (Kleywegt & Jones, 1998) for the solute molecules. The final R value was 0.155 and $R_{\rm free}$ was 0.185. Refinement parameters are summarized in Table 1. Additional refinement information is contained in the PDB deposition 1y9a.

3. Results and discussion

3.1. Monomer structure

The monomer of EhADH consists of 360 residues and a catalytic zinc ion (Fig. 1*a*). The overall fold of the monomer is nearly identical to that of the previously determined structures of the homologous CbADH, TbADH, SsADH and PaADH. EhADH is divided into two well defined domains: the catalytic domain and the cofactor-binding domain. They are separated by a deep cleft into which the cofactor and substrate would be bound to the enzyme. At the bottom of this cleft is the catalytic domain (residues 1–155 and 294–360); the catalytic zinc is coordinated by the triad Cys37, His59 and Asp150. The

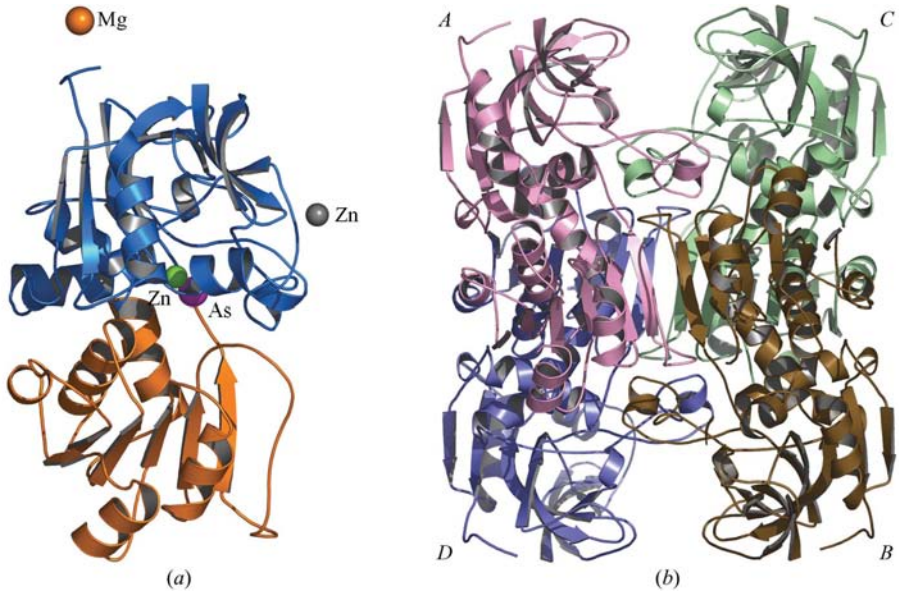

Figure 1
(*a*) Cartoon diagram of the EhADH monomer. The cofactor-binding domain is shown in blue and the catalytic domain in yellow. The catalytic zinc is shown as a CPK model in green; the packing zinc is in grey. The As of the bound cacodylate is shown in magenta and an Mg bound to the C-terminus is shown in orange. This figure was rendered using *MOLSCRIPT* (Kraulis, 1991). (*b*) The full tetramer of EhADH is generated by application of the crystallographic symmetry. The individual monomers are coloured as follows: monomer *A*, pink; symmetry-related monomer *B*, brown. Monomer *C* is green and its symmetry-related monomer *D* is blue. This figure was rendered using *PyMOL* (DeLano, 2002).

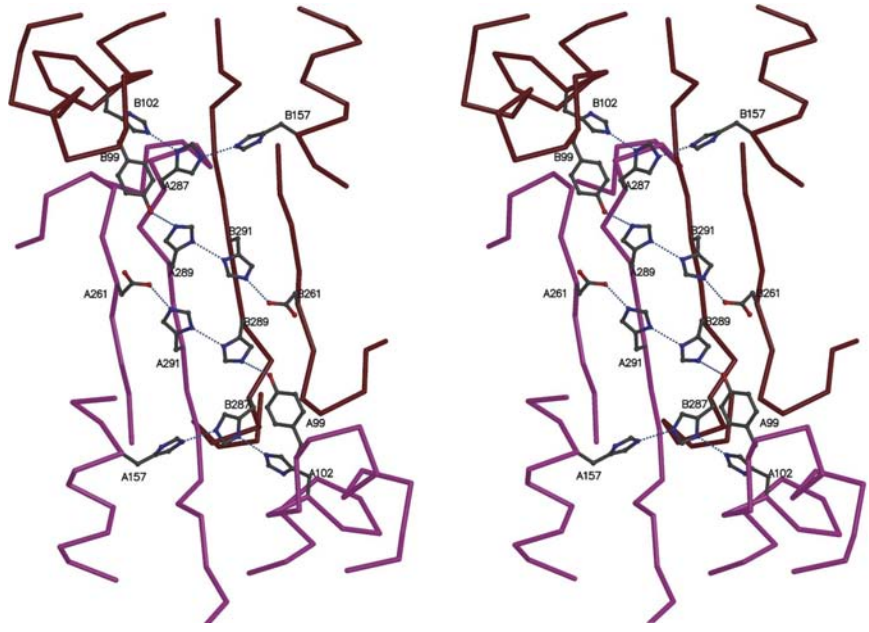

Figure 2
Stereo representation of the interface of the *A* and *B* monomers. The C^{α} backbone of monomer *A* is in pink and the C^{α} backbone of monomer *B* is in brown. Residues that form the hydrogen bonds of the 'histidine ladder' are labelled. This figure was rendered using *MOLSCRIPT* (Kraulis, 1991).

catalytic domain primarily has mixed β-sheet sandwich topology and is characterized by a 'protruding loop' (residues 87–109) with a short helical segment and an additional but non-catalytic Zn atom (Fig. 1*a*). The cofactor-binding domain (residues 156–293) folds with the α/β Rossmann-fold motif (Rossmann *et al.*, 1974) and is composed of a six-stranded parallel β-sheet packed against five α-helices, with two α-helices above and two α-helices below. The fifth α-helix is a long curved α-helix that packs against the side of the β-sheet and connects the cofactor-binding domain with the catalytic domain and can be considered as forming a flexible hinge between the two domains.

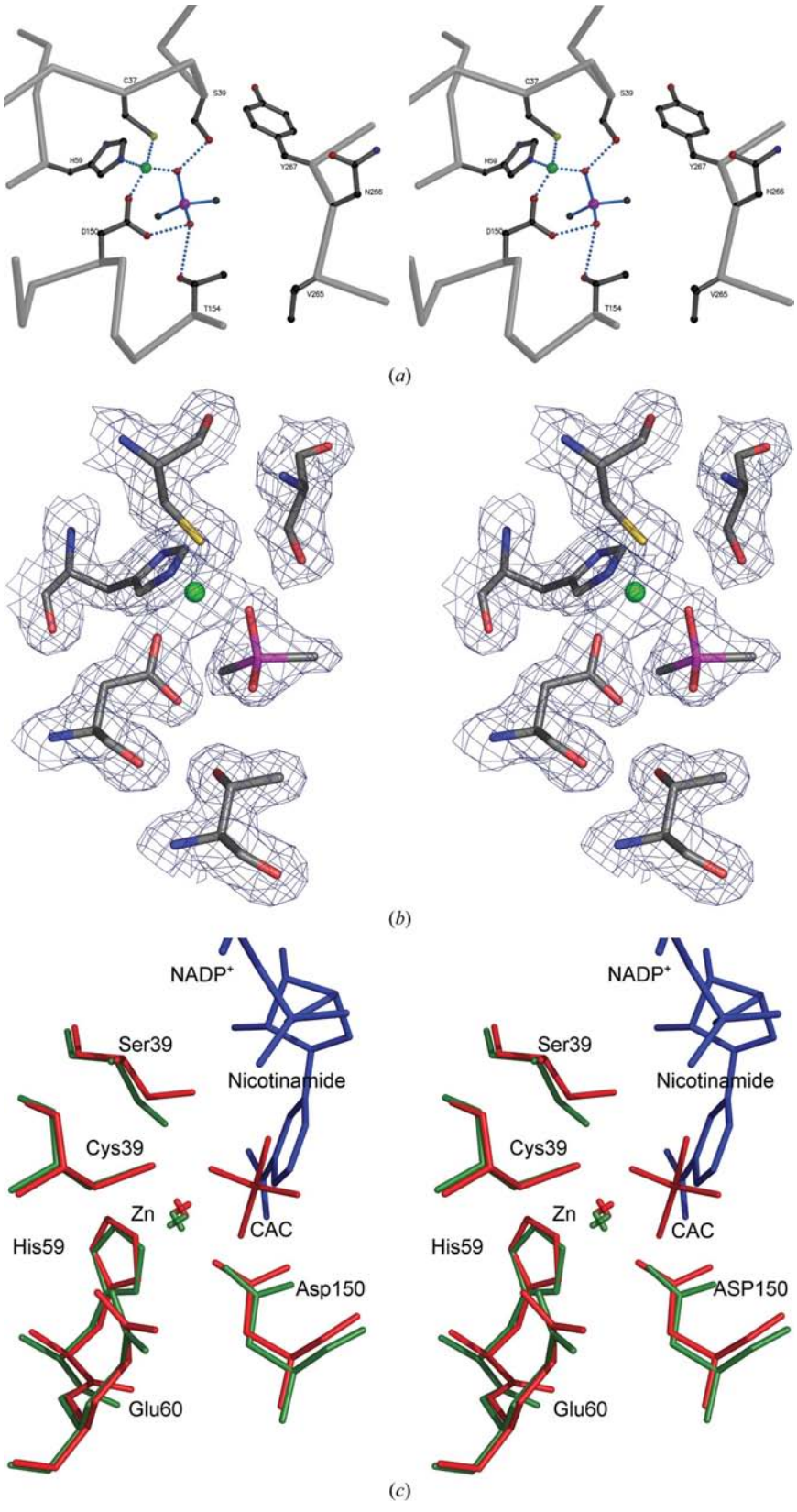

Superposing the structure of EhADH with the four independent monomers found in the asymmetric unit of CbADH (PDB code 1ped) results in r.m.s. deviations in C^{α} positions of 0.82, 0.82, 0.81 and 0.82 Å for monomer *A* of EhADH and 0.92, 0.91, 0.92 and 0.91 Å for monomer *C*. These superpositions were performed over residues 1–350 of CbADH and the corresponding residues of EhADH (the are no insertions or deletions within this range; however, EhADH has a C-terminus that is extended by ten residues). Similarly, superposition of EhADH with the four monomers found in the asymmetric unit of TbADH (PDB code 1ykf) results in r.m.s. deviations in C^{α} positions of 0.73, 0.73, 0.74 and 0.74 Å for monomer *A* of EhADH and 0.78, 0.78, 0.79 and 0.79 Å for monomer *C*. These superpositions were performed over residues 1–360 of TbADH, which the proteins have in common. A comparison of the two independent monomers within the EhADH asymmetric unit gives an r.m.s. deviation on 360 C^{α} positions of 0.44 Å.

3.2. Quaternary structure

EhADH is a homotetramer with approximate 222 symmetry. It may be regarded of as a dimer of dimers in which each dimer is highly similar to the dimeric ADHs. The individual monomers are organized as in bacterial and archeal ADHs and have been denoted *A*, *B*, *C* and *D* in accordance with

Figure 3
Catalytic pocket. (*a*) Stereo representation of the catalytic pocket. The catalytic Zn is in green and the As of the cacodylate molecule is in magenta. This figure was rendered using *MOLSCRIPT* (Kraulis, 1991). (*b*) Stereo representation of $2F_o - F_c$ electron density contoured at 1.0σ in the vicinity of the Zn, cacodylate and surrounding residues. This figure was rendered using *PyMOL* (DeLano, 2002). (*c*) Stereo representation of the superposition of the catalytic pockets of EhADH (red) and the holoenzyme structure of CbADH (green; PDB code 1kev). The $NADP^+$ of the CbADH is shown in blue and demonstrates that the position of cacodylate in the pocket would block the cofactor.

the naming of the monomers following the convention of the CbADH structure (Fig. 1*b*). The EhADH asymmetric unit contains a dimer designated *AC* and the biologically active tetramer is generated by crystallographic twofold symmetry. The second type of dimer designated *AB* (monomer *A* with its crystallographically related mate) has crystallographic twofold symmetry and the intersubunit contacts for these dimers take place along β-strands. This dimer interface packs one six-stranded parallel β-sheet of the cofactor-binding domain against another *via* the crystallographic twofold axis, thereby forming a continuous 12-stranded β-sheet that extends the full width of the tetramer.

The dimerization interface of these monomers is both extensive and extremely interesting. The six-stranded parallel β-sheet of the coenzyme-binding domain is positioned by the twofold axis abutting its symmetry equivalent, leading to the formation of an extended 12-stranded β-sheet running along of the tetramer internal cavity surface (Fig. 1*b*). The β–β interface is eight residues in length and comprises an extended network of hydrogen bonds between residues on either of the monomers and including three solute molecules of ethylene glycol, polyethylene glycol and incorporated water molecules. The β-strand to β-strand interactions are comprised of ten histidine residues arranged in four pairs plus one, which make direct hydrogen-bonding interactions forming a type of extended 'histidine ladder' (Fig. 2). In addition, hydrogen bonds between main-chain oxygen to main-chain nitrogen make the β-sheet connections. A second antiparallel β-sheet–β-sheet interface surface is found on the exterior solvent-facing surface of the tetramer. These interactions are presented in Table 2. To the best of our knowledge, this type of histidine arrangement appears to be a novel motif, as a structure-based search of the PDB could find no similar pattern.

In the tetrameric molecule of EhADH, 22% of the total accessible surface of the protein is involved in crystal contacts. The solvent-excluded surface of the entire tetramer is 13 514 Å^2. In the first type of dimer, the non-crystallographic *AC* dimer discussed above, the dimer-interface region is limited and the total buried surface area is 1653 Å^2. The more extensive β–β interaction of the *AB* dimer has a total excluded area of 3878 Å^2.

3.3. The catalytic site

The catalytic site of the enzyme is found in the deep cleft that separates the catalytic domain and the cofactor-binding domain. It is built of a catalytic Zn atom (Figs. 3*a* and 3*b*) that is tetrahedrally coordinated to Cys37 S^{γ}, His59 $N^{\varepsilon 2}$ and Asp150 $O^{\delta 2}$ with distances of 2.33, 2.06 and 1.98 Å, respectively, which are within the expected distances for metal-

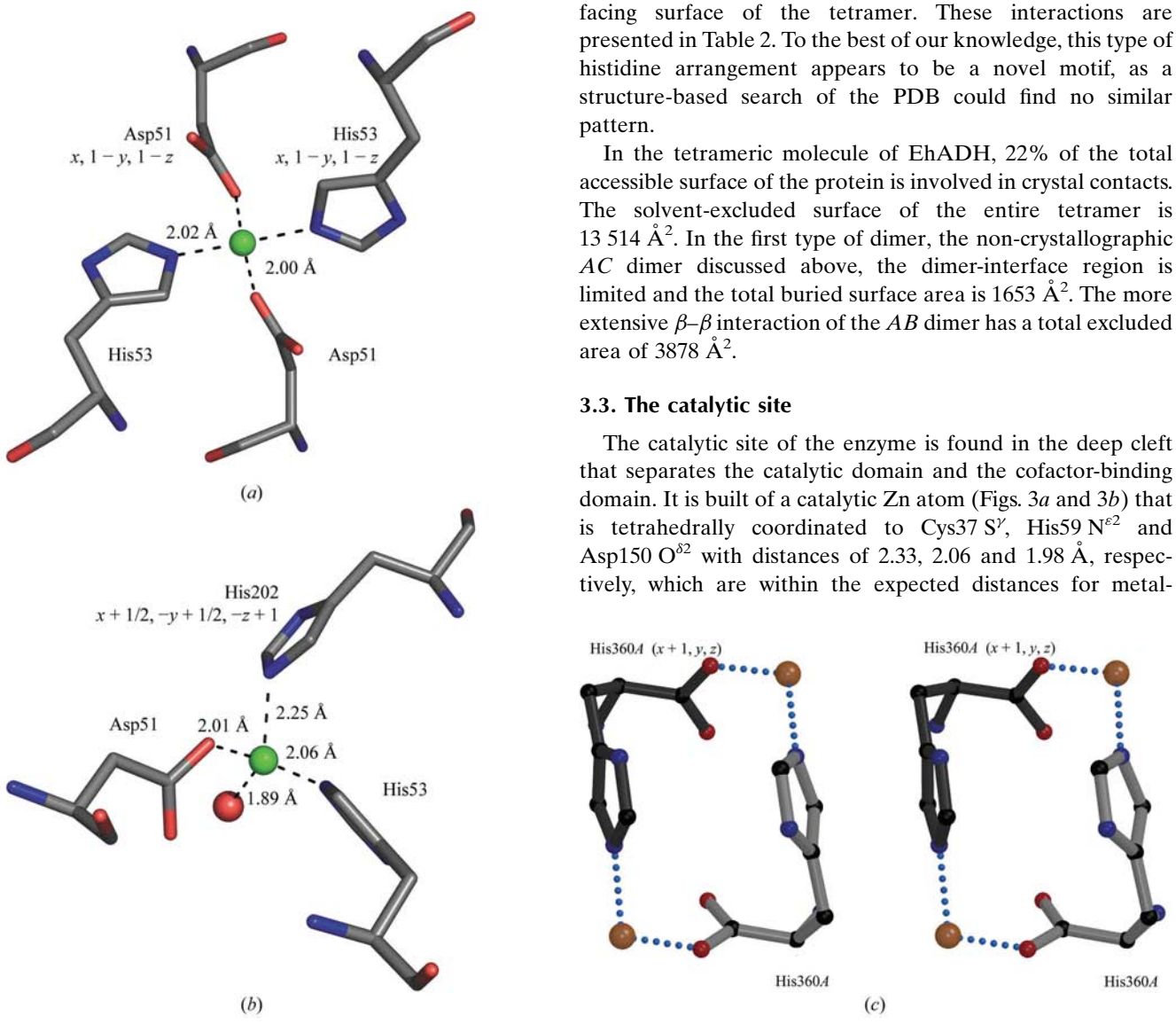

Figure 4
Packing interactions. (*a*) Representation of the Zn-mediated packing interaction between monomer *C* and a symmetry-related (x, $-y + 1$, $-z + 1$) *C* monomer of an adjacent tetramer. This figure was rendered using *PyMOL* (DeLano, 2002). (*b*) Representation of the analogous Zn-mediated interaction in monomer *A*. The symmetry-related molecule is the monomer *C* ($x + 1/2$, $-y + 1/2$, $-z + 1$). The crystallographic dyad does not coincide with the Zn and the interactions are not with the symmetry-equivalent residues. This figure was rendered using *PyMOL* (DeLano, 2002). (*c*) Stereo representation of the Mg-mediated His–His interaction at the C-terminus of monomer *A*. No analogous interaction is made within monomer *C*. This figure was rendered using *MOLSCRIPT* (Kraulis, 1991).

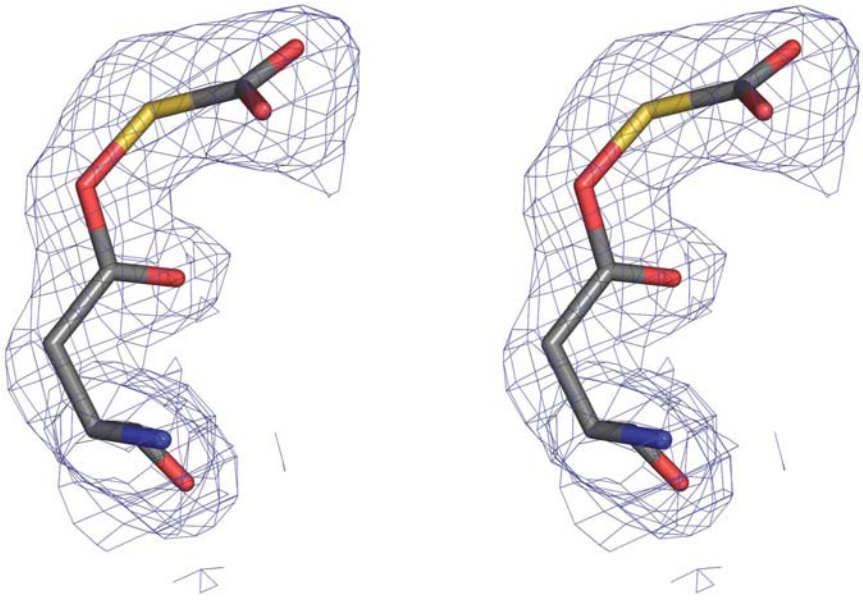

Figure 5
Stereo representation of the $2F_o - F_c$ electron density contoured at 1.0σ at residue 245, demonstrating the modification of the side chain. This figure was rendered using *PyMOL* (DeLano, 2002).

coordination groups in proteins (Harding, 2004). The fourth ligand in this tetrahedral coordination is an O atom from a cacodylate molecule that is adjacent to the active site. The cacodylate molecule is well defined and exhibits tetrahedral geometry (Figs. 3*a* and 3*b*). It occupies the position which would normally be held by the nicotine amide moiety of the cofactor, apparently blocking the active site of the enzyme (Fig. 3*c*). It is connected to the catalytic zinc *via* one of the O atoms, with a bonding distance of 1.98 Å. The second of the two O atoms makes a hydrogen bond of 2.61 Å to Asp150 $O^{\delta1}$. The two methyl groups of the cacodylate molecule do not appear to participate in any direct contacts and point into a small hydrophobic pocket lined by Ile86, Trp110 and Cys285. The distances given above are for monomer *A* and are nearly identical in monomer *C*.

In the previously determined structures from the related homologues of TbADH (PDB code 1ykf) and CbADH (1ped, 1kev), this O atom came from residue Glu60. This Glu is conserved in EhADH and could theoretically have been the fourth Zn ligand. In the current structure, Glu60 is 4.31 Å from the Zn and makes bifurcated hydrogen bonds of 2.77 and 3.04 Å to Lys346.

3.4. Crystal-packing contacts

In addition to the cacodylate molecules, the composition of the crystallization solute has resulted in the crystallographic modelling of two additional zinc ions that participate in crystal-packing interactions, magnesium and acetate ions, as well as five ethylene glycol molecules per asymmetric unit dimer. In spite of the molecular equivalence of the two independent monomers, each has a distinctive crystal environment as they are related to each other by local non-crystallographic symmetry alone.

The non-catalytic Zn associated with monomer *C* sits on a crystallographic twofold axis. It lies at the centre of a distorted tetrahedron, coordinated by His53 and Asp51 of monomer *C* and His53 and Asp51 of *C*′, where *C*′ is a symmetry-related monomer on an adjacent tetramer (Fig. 4*a*).

The corresponding Zn associated with monomer *A* sits in a different crystal environment. While still coordinated by His53 and Asp51 of monomer *A*, crystal packing brings it into close proximity of His202 of a symmetry-related monomer *C*″ in a neighbouring tetramer; the fourth ligand is water (Fig. 4*b*). These interfaces are crystallographically non-equivalent and as such the resulting Zn coordination spheres are different; however, crystal-packing considerations in combination with the amino-acid sequence have resulted in two well defined Zn-binding sites.

One Mg ion is found at the C-terminus of monomer *A*, causing the formation of an intricate packing contact. It binds to His360 in such a way that the residue is stacked against its crystallographically symmetry-related counterpart belonging to a neighbouring tetramer, with a stacking distance of 3.56 Å (Fig. 4*c*). An unusual modification was seen at residue 245 in both independent monomers *A* and *C*; Asp245 has been converted to *O*-carboxysulfanyl 4-oxo-L-homoserine (denoted OHS in the PDB file 1y9a) by the addition of S-COOH to $O^{\delta2}$. The source and biological significance of this modification is currently unknown and is now under investigation; however, the electron density in this region is clear and makes its identification possible (Fig. 5).

We thankfully acknowledge the ESRF for synchrotron beam time and staff scientists of the ID14 stations cluster for their assistance. This work was supported by the Israel Science Foundation (ISF Research Grant No. 296-00 to YB).

References

Bogin, O., Peretz, M., Hacham, Y., Korkhin, Y., Frolow, F., Kalb (Gilboa), J. A. & Burstein, Y. (1998). *Protein Sci.* **7**, 1156–1163.
Brünger, A. T., Adams, P. D., Clore, G. M., DeLano, W. L., Gros, P., Grosse-Kunstleve, R. W., Jiang, J.-S., Kuszewski, J., Nilges, M., Pannu, N. S., Read, R. J., Rice, L. M., Simonson, T. & Warren, G. L. (1998). *Acta Cryst.* D**54**, 905–921.
Collaborative Computational Project, Number 4 (1994). *Acta Cryst.* D**50**, 760–763.
Danielsson, O., Atrian, S., Luque, T., Hjelmqvist, L., Gonzalezduarte, R. & Jornvall, H. (1994). *Proc. Natl Acad. Sci. USA*, **91**, 4980–4984.
DeLano, W. L. (2002). *The PyMOL Molecular Graphics System.* DeLano Scientific, San Carlos, CA, USA. http://www.pymol.org.
Eklund, H., Nordstrom, B., Zeppezauer, E., Soderlund, G., Ohlsson, I., Boiwe, T., Soderberg, B., Tapia, O., Branden, C. & Akeson, A. (1977). *J. Mol. Biol.* **102**, 27–59.

Emsley, P. & Cowtan, K. (2004). *Acta Cryst.* D**60**, 2126–2132.
Engh, R. A. & Huber, R. (1991). *Acta Cryst.* A**47**, 392–400.
Esposito, L., Sica, F., Raia, C. A., Giordano, A., Rossi, M., Mazzarella, L. & Zagari, A. (2002). *J. Mol. Biol.* **318**, 463–477.
Goihberg, E. (2001). MSc Thesis. Feinberg Graduate School, Weizmann Institute of Science, Israel.
Guy, J. E., Isupov, M. N. & Littlechild, J. A. (2003). *J. Mol. Biol.* **331**, 1041–1051.
Harding, M. M. (2004). *Acta Cryst.* D**60**, 849–859.
Jones, T. A., Zou, J. Y., Cowan, S. W. & Kjeldgaard, M. (1991). *Acta Cryst.* A**47**, 110–119.
Karlsson, A., El-Ahmad, M., Johansson, K., Shafqat, J., Jornvall, H., Eklund, H. & Ramaswamy, S. (2003). *Chem. Biol. Interact.* **143**, 239–245.
Kleywegt, G. J. & Jones, T. A. (1998). *Acta Cryst.* D**54**, 1119–1131.
Korkhin, Y., Kalb, A. J., Peretz, M., Bogin, O., Burstein, Y. & Frolow, F. (1998). *J. Mol. Biol.* **278**, 967–981.
Kraulis, P. J. (1991). *J. Appl. Cryst.* **24**, 946–950.
Lamzin, V. S., Perrakis, A. & Wilson, K. S. (2001). *International Tables for Crystallography*, Vol. *F*, edited by M. G. Rossmann & E. Arnold, pp. 720–722. Dordrecht: Kluwer Academic Publishers.
Lamzin, V. S. & Wilson, K. S. (1993). *Acta Cryst.* D**49**, 129–147.
Laskowski, R. A., MacArthur, M. W., Moss, D. S. & Thornton, J. M. (1993). *J. Appl. Cryst.* **26**, 283–291.
Levin, I., Meiri, G., Peretz, M., Burstein, Y. & Frolow, F. (2004). *Protein Sci.* **13**, 1547–1556.
Murshudov, G. N., Vagin, A. A. & Dodson, E. J. (1997). *Acta Cryst.* D**53**, 240–255.
Navaza, J. (1994). *Acta Cryst.* A**50**, 157–163.
Otwinowski, Z. & Minor, W. (1997). *Methods Enzymol.* **276**, 307–326.
Peretz, M., Bogin, O., Tel-Or, S., Cohen, A., Li, G. S., Chen, J. S. & Burstein, Y. (1997). *Anaerobe*, **3**, 259–270.
Pietruszko, R. (1975). *Adv. Exp. Med. Biol.* **56**, 1–31.
Potterton, E., Briggs, P., Turkenburg, M. & Dodson, E. (2003). *Acta Cryst.* D**59**, 1131–1137.
Rossmann, M. G., Moras, D. & Olsen, K. W. (1974). *Nature (London)*, **250**, 194–199.
Samuelson, J., Zhang, W. W., Kumar, A., Descoteaux, S., Shen, P. S. & Bailey, G. (1992). *Arch. Med. Res.* **23**, 31–33.
Sheldrick, G. M. & Schneider, T. R. (1997). *Methods Enzymol.* **277**, 319–343.
Shimon, L. J. W., Peretz, M., Goihberg, E., Burstein, Y. & Frolow, F. (2002). *Acta Cryst.* D**58**, 546–548.
Vriend, G. (1990). *J. Mol. Graph.* **8**, 52–56.
Winn, M. D., Murshudov, G. N. & Papiz, M. Z. (2003). *Methods Enzymol.* **374**, 300–321.